

# Analysis of quantum effects in non-uniformly doped MOS structures

Claudio Fiegna and Antonio Abramo<sup>◊</sup>

Dept. of Engineering, Univ. of Ferrara

Via Saragat 1, 44100 Ferrara, Italy

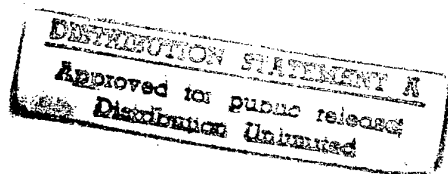
Phone: +39-532-293832, FAX: +39-532-768602

<sup>◊</sup> INFN, Dept. of Physics, Univ. of Modena

September 23, 1997

## Abstract

This paper presents results from the self-consistent solution of Schrödinger and Poisson equations obtained in one-dimensional non-uniformly doped MOS structures suitable for the fabrication of very short transistors. Different issues are considered and investigated, including quantum-induced threshold voltage shifts, low-field electron effective mobility and gate-to-channel capacitance. The reported results give indications for the optimization of n-MOS channel doping profiles suitable for the fabrication of ultra-short MOSFETs.



1  
DPO QUALITY INSPECTED 3

19971112 054

## Introduction

As it is well known, the MOSFET scaling theories (e.g. [1, 2]) give detailed prescriptions on how both physical dimensions and technological parameters should be changed to properly design short channel devices. In particular, high doping concentrations ( $\approx 10^{18}\text{cm}^{-3}$ ) and thin gate oxides ( $\approx 3\text{nm}$ ) are required to limit 2D short-channel effects (SCE) in ultra-short (US-) MOSFETs with gate length ( $L_G$ ) below  $0.1\text{ }\mu\text{m}$  [3].

At the Si-SiO<sub>2</sub> interface of MOS systems, electron energy quantization occurs. In the case of the earliest MOS technologies, its main consequence consisted in the reduction of low-field mobility with respect to bulk Silicon [4]. In modern technologies, the effects of quantization tend to become more relevant and easily detectable [5, 6, 7, 8]. In particular, high channel doping concentration is responsible for strong energy quantization that, in turn, causes quantum induced threshold voltage shift (Q-DV) [5, 6]. Furthermore, as the centroid of the charge distribution is displaced from the interface, gate capacitance reduces with respect to  $C_{OX} = \epsilon_{OX}/t_{OX}$  [7, 8], and such a reduction becomes more relevant as  $t_{OX}$  is scaled down and the channel doping is decreased.

Therefore, theoretical studies based on semi-classical models, aiming at the optimization of the channel doping profile [9], must be extended to account for the effects of energy quantization. Previous works have been devoted to the analysis, on a quantum basis, of the threshold voltage deviations caused by high dopings [5, 6], and to the effects of quantization on the inversion-layer capacitance [7, 8]. However, the considered devices did not feature extremely non-uniform channel doping profiles, like those obtainable by epitaxial techniques [10].

In this study, a self-consistent one-dimensional (1D) Poisson-Schrödinger solver [11] is used to determine the electrostatic behavior of devices featuring highly non-uniform doping profiles, which are more realistic for the fabrication of US-MOSFETs. As a case study, quantum effects in an epitaxial-channel (EPI) MOS structure are investigated. Since we are interested in the operation of MOSFETs at room temperature, all the simulations are performed at 300 K.

To compare the different channel doping profiles, three macroscopic quantities are

evaluated: i) the quantum-induced threshold voltage shift; ii) the electron low-field mobility; iii) the MOS capacitance, including the effect of charge displacement from the interface.

The obtained results put in evidence that quantum phenomena in MOS inversion layers are not simply related to doping values close the Si-SiO<sub>2</sub> interface, but a more complex relationship holds, involving the actual doping profile within a range of few tenths of a micron away from the interface. Furthermore, this study provides design guidelines for the optimization of channel doping profiles, to be traded-off with those related to 2D SCE.

The paper is organized as follows: Section 1 presents the simulated device structure, the adopted physical models, and the numerical techniques used in this study; Section 2 presents the simulation results. Finally, Section 3 summarizes the conclusions of this work.

## 1 Simulated structure and methodology

In this work, we simulated a one-dimensional MOS capacitor featuring an ideal doping profile, as could be obtained by epitaxial growth. A low-doped EPI (with doping concentration  $N_{EPI}$  and thickness  $t_{EPI}$ ) covers a highly doped region (doping concentration  $N_A$ ) acting as a background plane to suppress punch-through. The purpose of the surface layer is to improve low-field mobility by reducing the transverse electric field (TEF) (i.e. surface roughness scattering) and the effect of ionized impurities. Since we are investigating a possible structure for MOS devices with  $L_G \leq 0.1 \mu\text{m}$ , we assumed very thin oxide (typically  $t_{OX}=3 \text{ nm}$ ) and epitaxial-layer thicknesses ( $t_{SI}$  as thin as 10 nm). Fig.1 reports the diagram of the conduction band across the MOS structure and the first 20 quantized energy levels self-consistently computed for the case  $t_{OX}=3 \text{ nm}$ ,  $t_{EPI}=10 \text{ nm}$   $N_A=1 \times 10^{18} \text{ cm}^{-3}$ ,  $N_{EPI}=1 \times 10^{15} \text{ cm}^{-3}$ , inversion electron sheet concentration  $N_S=3 \times 10^{12} \text{ cm}^{-2}$ .

As said, the issues of Q-DV, low-field electron effective mobility and gate-to-channel

capacitance have been investigated by a one-dimensional approach. Therefore, the results obtained are valid for low applied drain-to-source voltages, i.e. in the linear MOSFET regime, or, more in general, when two-dimensional effects can be assumed to be small. Despite to this limitation, the results of this paper are anyway valid as a comparison between the different doping solutions analyzed. In fact, since the concept of "short MOSFET" (i.e. suffering of relevant 2D short channel effects) is relative to the adopted technology, even a 0.1 micron MOSFET fabricated with a 50 nm technology and operating at low voltages [3], can be considered as a "long channel" device. Therefore, for such a device 1D results are relevant.

The simulations were carried out by self-consistently solving the Poisson and Schrödinger equations with a Gummel-like iteration [11]. The envelope function equation (i.e. Schrödinger equation in the effective mass approximation) is solved to determine the eigenvalues and eigenvectors of the system. In this solution, the six-fold ellipsoidal symmetry is assumed for the silicon, with the usual values for longitudinal and transverse masses (0.19 and 0.915 in free electron mass units, respectively), together with a parabolic energy vs.  $k$ -vector dispersion relationship, adequate for the case of n-channel MOS structures [12]. A zero wave function boundary condition is forced at the quantum system boundaries, i.e. in the substrate and at the oxide interface. Therefore, wave function penetration into the oxide is neglected.

From the numerical point of view, the solution is determined in the frame of the finite elements formalism, solving the generalized eigenproblem using the inverse iteration, Rayleigh-quotient, and Gram-Schmidt algorithms.

Once the eigenstates are determined, the quantum electron density and the classical hole density are computed using Fermi-Dirac and Maxwell-Boltzmann statistics, respectively. Complete ionization of the dopant is also assumed.

## 2 Simulation Results

In this Section we report the simulation results related to energy quantization inside the channel of an EPI device. For the sake of clarity, the discussion has been organized into three subsections, dealing with threshold voltage, effective mobility, and gate capacitance effects, respectively.

### 2.1 Threshold voltage results

We have simulated the EPI structure with  $t_{EPI}$  down to 10 nm and  $t_{OX}$  down to 3 nm, investigated in [9] for application to MOSFETs with  $L_G$  down to 50 nm. Its threshold voltage ( $V_{TH}$ ), computed as the linear extrapolation of the simulated quantum inversion charge  $Q_S$  vs. voltage characteristic, has been studied. In particular, we focused on the threshold voltage shift with respect to the classical solution (i.e. the Q-DV) for the EPI structure and for the more conventional highly doped (UHD) structure obtained setting  $t_{EPI}=0$ . Due to the low surface doping, a much lower Q-DV could be expected in the EPI case compared to UHD. Instead, similar Q-DV is obtained for UHD and EPI with small  $t_{EPI}$ . In fact, for  $t_{EPI}=10$  nm and  $t_{OX}$  ranging from 3 to 10 nm, we obtained only a 20% reduction of Q-DV with respect to UHD, showing that this effect does not simply depend on the doping at the interface, but rather, a long-range dependence on doping holds. This point is emphasized by Fig.2-a, where Q-DV is reported as a function of  $t_{EPI}$ : a relatively thick EPI is needed to eliminate the quantum effects originated by the presence of the high-doped background plane. Fig.2-b, instead, shows how  $V_{TH}$  can be controlled by properly selecting  $t_{EPI}$ : while the UHD MOS presents a threshold voltage that is too large for low supply voltage applications ( $V_{DD} \approx 1-1.5$  V) the introduction of the low-doped layer provides a further degree of freedom, additional to the doping of the background-plane, for designing the threshold voltage according to circuit applications. The reported results clearly show that simple Q-DV models based on average channel doping values cannot be applied to the highly non-uniform cases needed for US-MOSFETs.

## 2.2 Effective mobility results

We can address channel electron effective mobility starting from Fig.3. showing the profiles of the quantum electron density in structures that feature  $N_A=1\times 10^{18} \text{ cm}^{-3}$ ,  $N_{EPI}=1\times 10^{15} \text{ cm}^{-3}$ ,  $t_{OX}=3\text{nm}$ , and different  $t_{EPI}$ . The comparison between different structures has been performed for a given inversion sheet density above threshold ( $N_S=3\times 10^{12} \text{ cm}^{-2}$ ). For increasing  $t_{EPI}$  charge confinement reduces due to the reduction of transverse electric field. Consequently, an improved effective mobility ( $\mu_{\text{eff}}$ ) shall be expected for larger  $t_{EPI}$ .

In fact, the introduction of low-doped EPI effectively decreases the effective electric field (EEF), reported in Fig.4 as a function of  $t_{EPI}$  for a given above-threshold inversion sheet density. Here, the EEF has been computed as the mean value of the electric field component normal to the interface averaged over the carrier density.

The corresponding  $\mu_{\text{eff}}$ , extracted from universal mobility curves [4] is also given in Fig.4, confirming what anticipated. It should be mentioned that the UHD device is expected to present even larger disadvantages for low inversion charge densities [4], due to the reduced screening of the Coulomb scatterers.

Additional results (Fig. 5) show that a lower effective field is obtained for the EPI with respect to the UHD, also when the comparison is performed for the same gate drive (e.g.  $V_G-V_{TH}$ ), which is a very significant comparison in view of circuit applications.

## 2.3 Gate capacitance results

Another important issue relates to total MOS capacitance  $C_{TOT}$ , i.e. the series of the oxide capacitance  $C_{OX}=\epsilon_{OX}/t_{OX}$  and of the inversion layer capacitance  $C_{INV}=dQ_S/d\varphi_S$ ,  $\varphi_S$  being the Si-surface potential. As mentioned,  $C_{TOT}$  in quantized inversion layers reduces with respect to  $C_{OX}$  as  $t_{OX}$  is decreased, due to the larger effective oxide thickness consequent to the displacement of the inversion charge from the device interface. As shown in [7] for uniform channels, such a reduction becomes more relevant for

lower dopings. Consequently, compared to the UHD case a lower capacitance should be expected for the EPI one. Fig.6-a reports  $C_{TOT}=dQ_S/dV_G$  as a function of  $t_{OX}$ , for  $t_{EPI}=10$  nm and 0 nm. As can be seen, the capacitance degradation increases at thinner oxides, but no additional degradation occurs if thin low-doped EPI is introduced. As reported in Fig.6-b, the simulated results indicate that no serious degradation shall be expected by the application to US-MOSFETs, such as those described in [9], of EPI layers up to 30-40 nm. Results obtained by classical simulation accounting for Fermi-Dirac statistics are also reported. Degenerate statistics can only partially account for the capacitance attenuation occurring at thin gate oxides as already reported in [8], furthermore, classical simulation underestimates capacitance dependence on  $t_{EPI}$ .

### 3 Conclusions

In this work a self-consistent Schrödinger-Poisson simulator has been applied to the study of highly non-uniform doping profiles suitable for the fabrication of ultra-short MOSFETs. The obtained results prove that a non trivial dependence of quantum effects on the channel doping profile holds. The introduction of a low doped region at the device surface allows to tailor the threshold voltage according to circuit applications, where the use of high dopings would lead, instead, to threshold values too high for realistic applications. Furthermore, the presence of a low-doped epitaxial region produces a reduction of the electron effective field for a given charge sheet density and, therefore, improves the electron effective mobility. As for gate total capacitance, the displacement of the inversion charge from the silicon surface causes its reduction with respect to  $C_{OX}$ , but no significant additional degradation has been found as a consequence of the introduction of a low-doped epitaxial layer.

## Acknowledgements

One of the authors (A.A.) thanks A.R.O., O.N.R, and E.R.O. for partially funding the work.

## References

- [1] R.H. Dennard, F.H. Gaensslen, L. Kuhn, N.Y. Yu, V.L. Ridout, E. Bassous, and A. LeBlanc, "Design of ion-implanted MOSFETs with very small physical dimensions", *IEEE J. Solid State Circuits*, vol. 9, p. 256 (1974).
- [2] G. Baccarani, M.R. Wordeman, and R.H. Dennard. "Generalized scaling theory and its application to a 1/4 micrometer MOSFET design", *IEEE Trans. Electron Devices*, vol. 31, p.452 (1984).
- [3] M. Ono, M. Saito, T. Yoshitomi, C. Fiegna, T. Ohguro, and H. Iwai, "A 40 nm gate length n-MOSFET", *IEEE Trans. Electron Devices*, vol. 42, p. 1822 (1995).
- [4] S. Takagi, A. Toriumi, M. Iwase, and H. Tango, "On the universality of inversion layer mobility in Si MOSFET's: part I - effects of substrate doping concentration". *IEEE Trans. Electron Devices*, vol. 41, p. 2357 (1994).
- [5] M.J. van Dort, P.H. Woerlee, A.J. Walker, C.A.H. Juffermans, and H. Lifka, "Influence of high substrate doping levels on the threshold voltage and the mobility of deep-submicrometer MOSFET's", *IEEE Trans. Electron Devices*, vol. 39, p. 932 (1992).
- [6] S.A. Hareland, S. Krishnamurthy, S. Jallepalli, C. Yeap, K. Hasnat, A.F. Tash Jr., C.M. Maziar, "A computationally efficient model for inversion layer quantization effects in deep submicron n-channel MOSFET's", *IEEE Tran. Electron Devices*, vol. 43, p. 90 (1996).
- [7] S. Takagi, and A. Toriumi, "Quantitative understanding of inversion-layer capacitance in si MOSFET's", *IEEE Trans. Electron Devices*, vol. 42, p. 2125 (1995).

- [8] K.S. Krish, J.D. Bude, and L. Manchanda, "Gate capacitance attenuation in MOS devices with thin gate dielectrics", *IEEE Electron Device Lett.*, vol. 11, p. 521 (1996).
- [9] C. Fiegna, H. Iwai, T. Wada, M. Saito, E. Sangiorgi, and B. Riccò, "Scaling the MOS transistor below 0.1  $\mu\text{m}$ : methodology, device structures and technology requirements", *IEEE Trans. Electron Devices*, vol. 41, p. 941 (1994).
- [10] M. Aoki, T. Ishii, T. Yoshimura, Y. Kiyota, S. Iijima, T. Yamanaka, T. Kure, K. Ohyu, T. Nishida, S. Okazaki, K. Seki, and K. Shimohigashi, "0.1  $\mu\text{m}$  CMOS devices using low-impurity-channel transistors (LICT)", in IEDM Tech. Dig., pp. 939-941, (1990).
- [11] A. Abramo, J. Bude, F. Venturi, and M.R. Pinto, "Mobility simulation of a novel Si/SiGeFET structure", *IEEE Electron Device Lett.*, vol. 17, p. 59 (1996).
- [12] S. Jallepalli, J. Bude, W.-K. Shih, M.R. Pinto, C.M. Maziar, and A.F. Tasch, Jr., "Electron and hole quantization and their impact on deep submicron silicon p- and n-MOSFET characteristics", *IEEE Trans. Electron Devices*, vol. 44, p. 297 (1997).

## Figure Captions

**Fig.1** Conduction band across the MOS structure Fermi level (dash-dotted line) and the first 20 quantized energy levels computed for the case  $t_{OX}=3\text{ nm}$ ,  $t_{EPI}=10\text{ nm}$ ,  $N_A=1\times 10^{18}\text{ cm}^{-3}$ ,  $N_{EPI}=1\times 10^{15}\text{ cm}^{-3}$ , inversion electron sheet concentration  $N_S=3\times 10^{12}\text{ cm}^{-2}$ . The Fermi energy is only 7 meV below the first eigenvalue.

**Fig.2** a) Quantum induced  $V_{TH}$  shift vs. EPI thickness; b)  $V_{TH}$  vs. EPI thickness.  $t_{OX}=3\text{ nm}$ ,  $N_{EPI}=10^{15}\text{ cm}^{-3}$ ,  $N_A=10^{18}\text{ cm}^{-3}$ .

**Fig.3** Electron density vs. position for different EPI thicknesses. Symbols are for visualization only and do not correspond to actual discretization points. The bias  $V_G$  was set in order to obtain the same charge sheet density for all structures.

**Fig.4** a) Effective electric field (squares, left) and effective mobility (circles, right) vs. EPI thickness. The bias  $V_G$  was set in order to obtain the same charge sheet density for all structures.

**Fig.5** Effective electric field for the uniform MOSFET (circles) and for the EPI MOS with  $t_{EPI}=30\text{ nm}$  vs. Gate Drive ( $V_G-V_{TH}$ ).

**Fig.6** a) Total capacitance vs. oxide thickness for  $t_{EPI}=0, 10\text{ nm}$ . Symbols: simulated results. Dashed-line:  $C_{OX}$ . b) Total capacitance vs.  $t_{EPI}$  for  $t_{OX}=3\text{ nm}$ . Circles: simulated results; crosses: results of classical simulation. Dashed-line:  $C_{OX}$ .

All simulated structures feature  $N_{EPI}=10^{15}\text{ cm}^{-3}$ ,  $N_A=10^{18}\text{ cm}^{-3}$ . The bias  $V_G$  was always set in order to obtain the same charge sheet density ( $N_S=3\times 10^{12}\text{ cm}^{-2}$ ) for all structures.

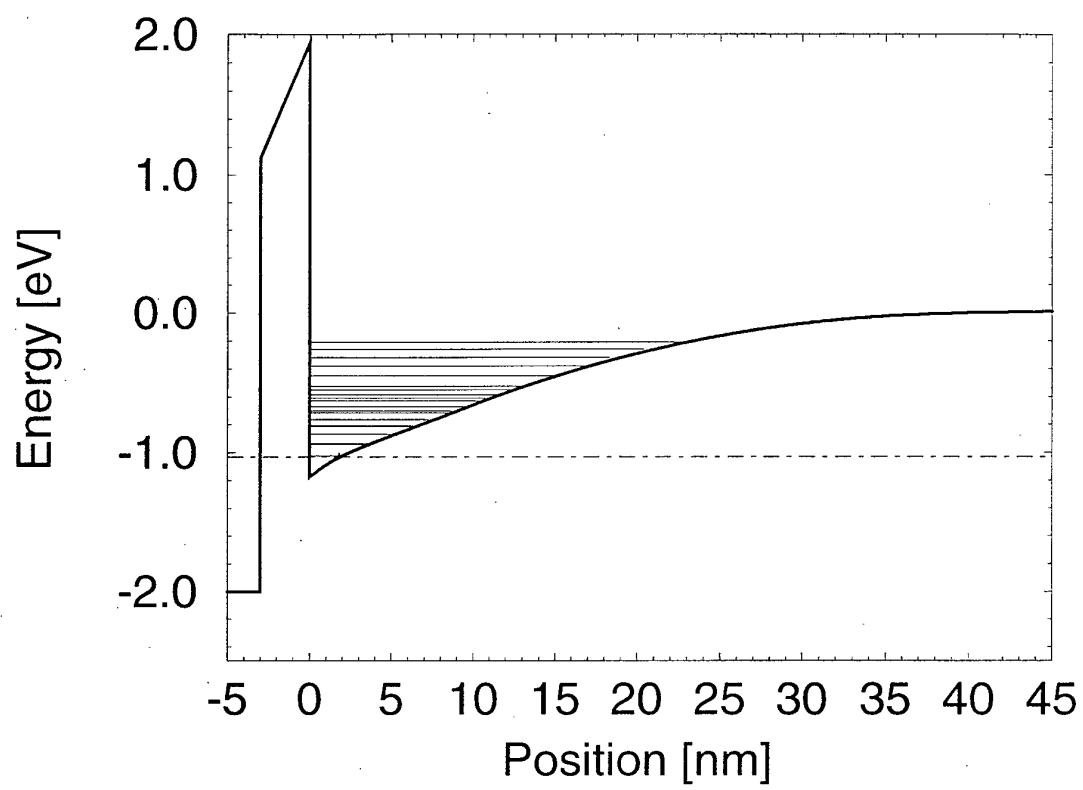


Figure 1:

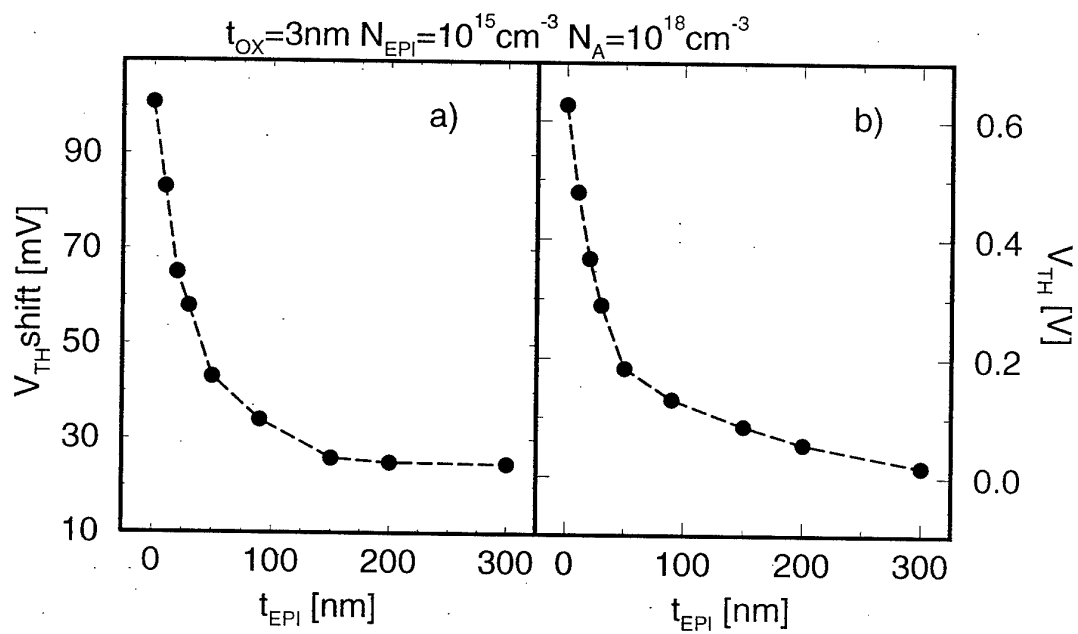


Figure 2:

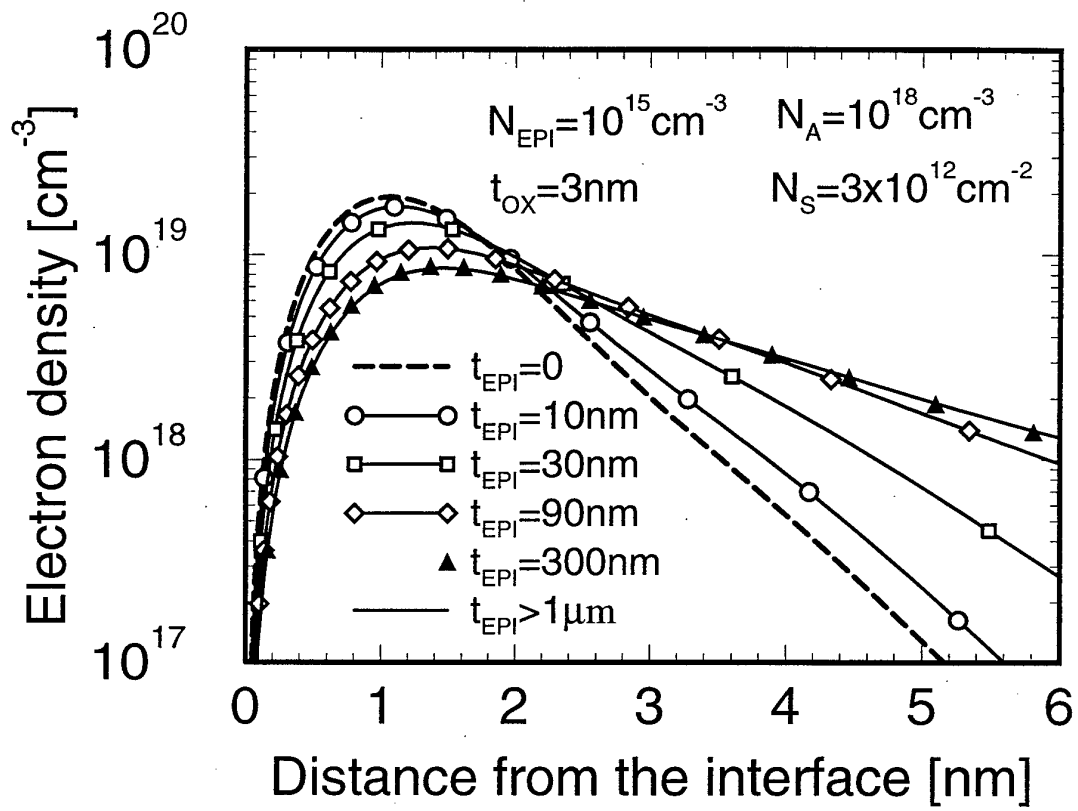


Figure 3:

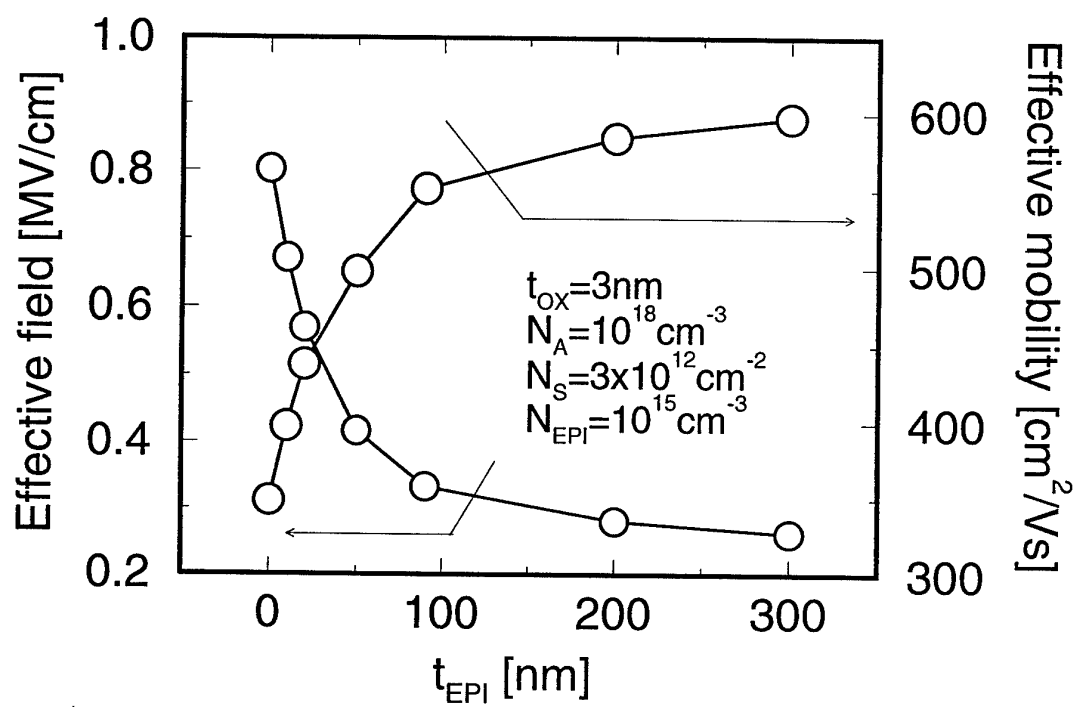


Figure 4:

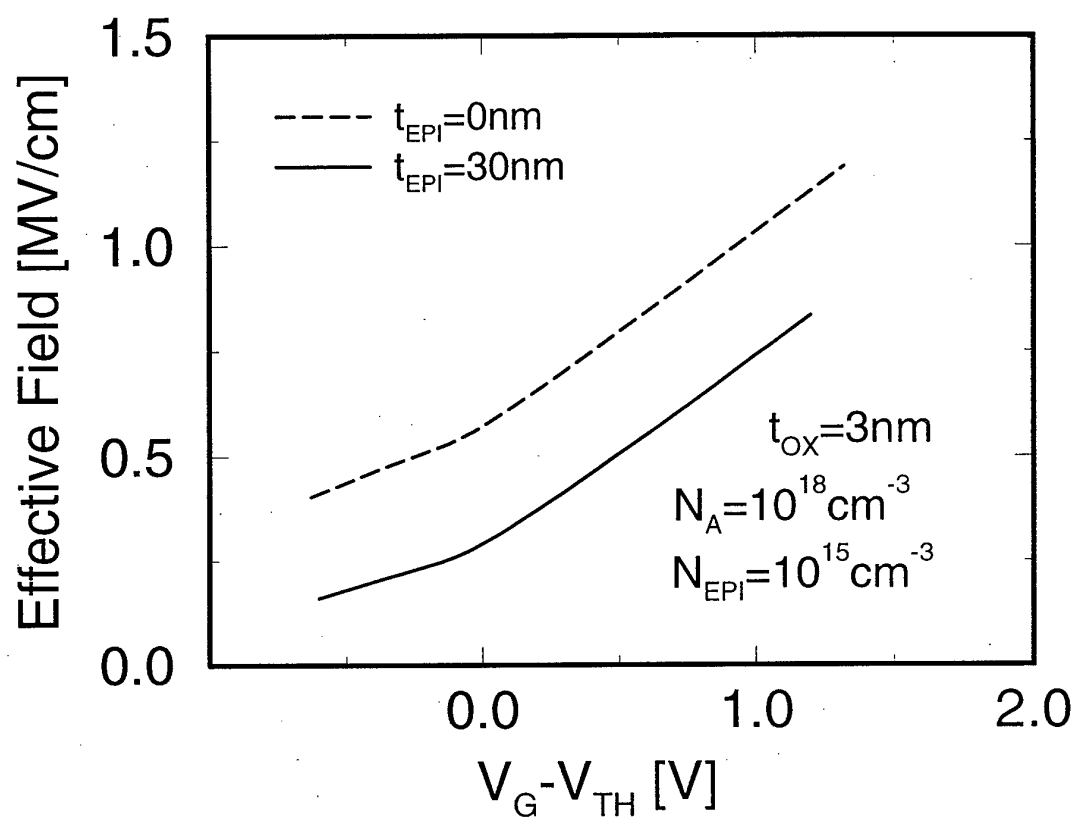


Figure 5:

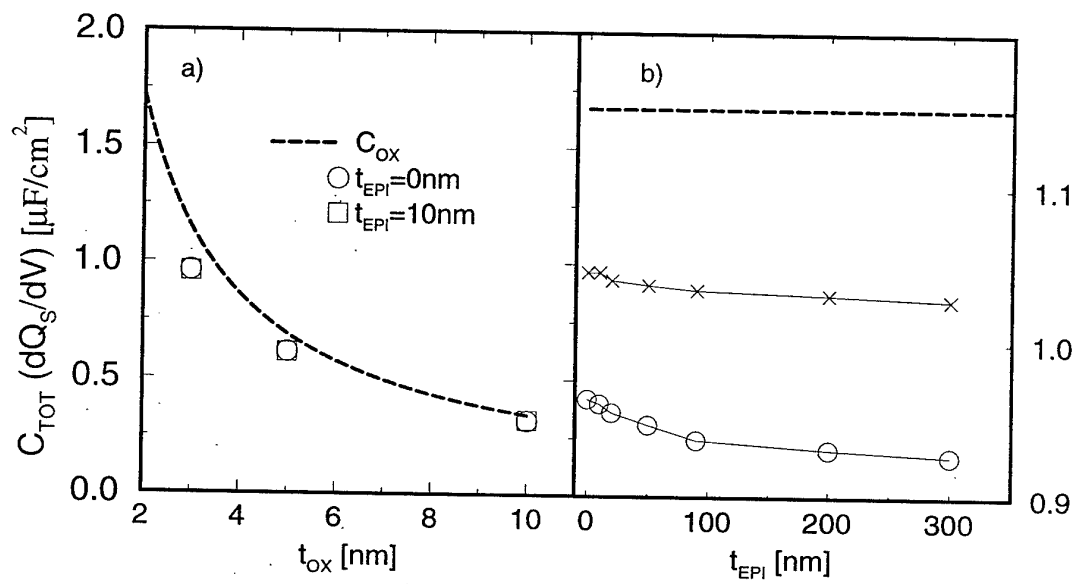


Figure 6: